JMEPEG (2012) 21:213–221
DOI: 10.1007/s11665-010-9816-9

1059-9495/$19.00

Electrochemical Deposition of Ni on an Al-Cu Alloy

A. Ul-Hamid, A. Quddus, H. Dafalla, H. Saricimen, and L. Al-Hadhrami

(Submitted May 11, 2010; in revised form August 25, 2010)

Metallic coatings can be used to improve the wear and corrosion resistance of Al alloys. In this study, Ni was used as a candidate material for such a coating which was applied on the surface of Al 2014 alloy using electrodeposition in a standard Watt's bath. A two-step heat treatment procedure was employed that served to increase the adhesion as well as hardness of Ni. Deposition was undertaken for different durations using both galvanostatic and potentiostatic techniques. The effect of deposition parameters such as surface finish, current, potential, temperature, pH level and duration on the microstructure, adhesion, and surface properties of the Ni deposit was studied. Materials characterization was performed using scanning electron microscopy, atomic force microscopy, and x-ray diffraction. Cross-sectional scanning transmission electron microscope images revealed the fine-grained (10 nm) structure of Ni initially deposited at the Ni-Al alloy substrate. Microhardness, adhesion, and corrosion behavior of the Ni deposit were evaluated. Experimental results indicate that deposition by galvanostatic technique on 1 μm surface finish at 45 °C with a pH level maintained at 3.6 represented the optimum conditions to generate a uniform Ni deposit on Al 2014. It was concluded that Ni deposition can be used to improve the surface properties of Al alloys.

Keywords Al alloy, corrosion, electrodeposition, microstructure, SEM

1. Introduction

Aluminum exhibits outstanding chemical stability under most atmospheric conditions due to rapid formation of a thin (≈1 nm) protective layer of alumina (Al_2O_3) at its surface. However, pure Al lacks adequate mechanical strength for structural applications. It is, therefore, combined with various alloying elements and heat treated to produce alloy grades with desired properties. Most alloying additions tend to lower the corrosion resistance of Al alloys. Both degree and nature of corrosion damage are greatly influenced by thermal treatment and the nature of Al alloy surface (Ref 1). Copper is a well-known alloying element in high-strength Al alloys and exists as $CuAl_2$ within the alloy matrix. Other alloying elements such as Mg and Si in addition to some Cr and Mn are also present as demonstrated by the 2014 alloy grade. Alloy 2014 is a heat treatable alloy with high fatigue strength and is used in high-strength structural applications such as aircraft fittings and wheels, military vehicles and bridges, forgings for trucks and machinery, weapons manufacture, etc. However, Al 2014 exhibits inadequate corrosion resistance in marine atmospheres and sea water necessitating the use of a surface protection system for Al 2014 (Ref 2).

Due to their low density and high thermal conductivity, Al alloys are also candidate materials for tribological applications such as in engine parts and sports products. In order to make them more suitable for these applications, surface of Al alloys need to become more resistant to mechanical as well as environmental degradation (Ref 3, 4). To enhance its corrosion and surface mechanical properties, surface of a high-strength Al alloy is generally coated using cladding, anodizing, and/or other protective layers.

Various techniques may be employed for surface protection including plasma and spray coating, welding, electrolytic and electroless coating, etc. Electrolytic and electroless coating are competitive techniques each with certain advantages. Electroless plating is usually more expensive than electroplating, and takes longer to produce a given thickness of coating deposit with accompanying waste disposal problems (Ref 5, 6). Nickel is used to improve surface properties of Al alloys for industrial applications such as Al automotive parts, wrought products, etc. In addition, electrodeposition of Ni has been employed to protect a range of materials for various applications (Ref 7–15).

This study was undertaken to determine the optimum electrolytic deposition conditions for Ni plating of high-strength Al 2014 alloy that can result in uniform and adherent deposits. The objective is to realize a basis for an alloy protection system that can potentially increase the capability of Al alloy for service in conditions that require enhanced resistance to environment and mechanical degradation. It was also the aim of this study to examine the microstructure formed at the interface of Al alloy substrate and Ni deposit.

2. Experimental Procedure

Nominal composition of Al 2014 alloy used for this study is shown in Table 1. Samples were prepared to 600 grit size and 1 μm diamond polished surfaces and degreased. They were immersed in zincate solution for 30 s followed by rinse in a solution that was prepared by mixing (3%) HNO_3 in (97%) methanol. Samples were dipped in zincate solution again and

A. Ul-Hamid, A. Quddus, H. Dafalla, H. Saricimen, and **L. Al-Hadhrami**, Center of Research Excellence in Corrosion, Research Institute, King Fahd University of Petroleum & Minerals, P.O. Box 1073, Dhahran 31261, Saudi Arabia. Contact e-mail: anwar@kfupm.edu.sa.

quickly introduced into Watt's plating solution for electrodeposition. Composition of Watt's bath and zincate solution used in this study is given in Table 2.

Electrodeposited samples were examined using scanning electron microscope (SEM-Model JEOL JSM 5900LV) coupled with Oxford ISIS energy dispersive spectroscopy (EDS). A scanning transmission electron microscope (STEM) detector mounted on FEI Helios NanoLab dual beam (FIB/SEM) was used to obtain cross-sectional images of Ni deposit. Atomic force microscopy (AFM-Model Agilent 5500) was used in contact mode to generate 10×10 μm^2 scans to study the surface topography of Ni deposits. X-ray diffractometer (Model- JEOL JDX 3530) with Cu Kα radiation was used to identify different phases present within the heat-treated samples.

Vickers microhardness tests were undertaken using a load of 200 g. Microscratch testing was conducted using a nanoindenter instrument (Model CSM Instruments NHT) fitted with a Rockwell diamond indenter having 100 μm tip radius at a final load of 30 N.

3. Results and Discussion

3.1 Effect of Electrodeposition Parameters on the Quality of Deposits

Pure Ni was used as an anode and Al 2014 as a cathode within the electrolytic bath to undertake electrodeposition at different plating conditions, as shown in Table 3. It was observed that current, voltage, bath temperature, pH, rate of stirring, and cathode surface finish, all affect the quality of electrodeposited Ni. Uniform, shining, and adherent deposits were obtained on samples with 1 μm surface finish when the bath solution pH was maintained at 3.6 with a constant current density of 50 mA/cm^2 at 45 °C for duration of 10 min (see low-magnification SEM micrograph in Fig. 1a). Higher than optimal temperature and stirring rate resulted in non-adherent and flaky deposits (see Fig. 1b), while lower temperature and stirring led to irregular and inconsistent deposits that failed to cover the entire surface of cathode (see Fig. 1c). Increased pH levels of the bath gave rise to cracked, flaky, and blackened deposits (see Fig. 1d). Samples with a 600 SiC grit size surface finish exhibited inconsistent and non-adherent deposits. It is believed that electrodeposition parameters mentioned above had a synergistic effect on the quality of deposits obtained. Temperatures away from the optimal value have an adverse effect on the activity of electrolyte solution and cathodic polarization. This degrades current efficiency and deposition rates affecting the ability to cover the entire cathode surface. At optimal conditions, the hydrogen evolution is believed to be minimal due to a decrease in polarization, giving best electrodeposition results. Lower than optimal pH values increase hydrogen evolution reaction generating hydrogen bubbles that cling to cathode surface and decrease the metal area available for Ni^{2+} reduction. This results in localized regions on the cathode surface devoid of Ni deposit. Increased pH can induce high degree of stresses within Ni deposit that can result in significant degradation of deposit morphology exhibiting cracking, curling, and darkening (Ref 16), as was observed in this study. Samples with 600 grit size finish exhibited greater surface roughness when compared to polished samples. It is relatively difficult to clean a rough surface and any microscopic non-metallic inclusion, such as oxide, dirt, grease, etc., settled on the surface can act as a pre-cursor for a void at the substrate-deposit interface giving rise to porosity. This adversely affects the adhesion of deposit resulting in its spallation at localized regions of the substrate.

Table 1 Nominal chemical composition of Al 2014 alloy

Elements	Chem. comp., wt.%
Al	Bal.
Cu	4.4
Fe	0.5
Mn	0.8
Si	0.8
Mg	0.4
Zn	0.25
Ti	0.15
Cr	0.10

Table 2 Composition of Watt's bath and zincate solution used in this study

Material	Amount
Watt's bath	
Nickel sulfate, g	125
Nickel chloride, g	22
Boric acid, g	15
Distilled water, L	0.5
Zincate solution	
Sodium hydroxide, g	263
Zinc oxide, g	50
Ferric chloride, g	0.5
Potassium sodium tartrate, g	5
Distilled water, L	0.5

Table 3 Different electroplating conditions used to obtain Ni deposits on samples with 1 μm surface finish

Plating conditions	Current, mA/cm^2	Voltage, V	Temperature, °C	pH	Observation
1	50	Variable	45	3.6	Best result, adherent consistent deposit
2	25	Variable	45	3.6	Inconsistent deposition
3	50	Variable	54	3.6	Flaky, non-adherent deposit
4	50	Variable	38	3.6	Irregular and inconsistent deposit
5	50	Variable	54	4.6	Cracked, flaky, non-adherent deposit
6	50	Variable	35	3.8	Blackened flaky non-adherent deposit
7	Variable	1.2	46	3.7	Inconsistent deposit

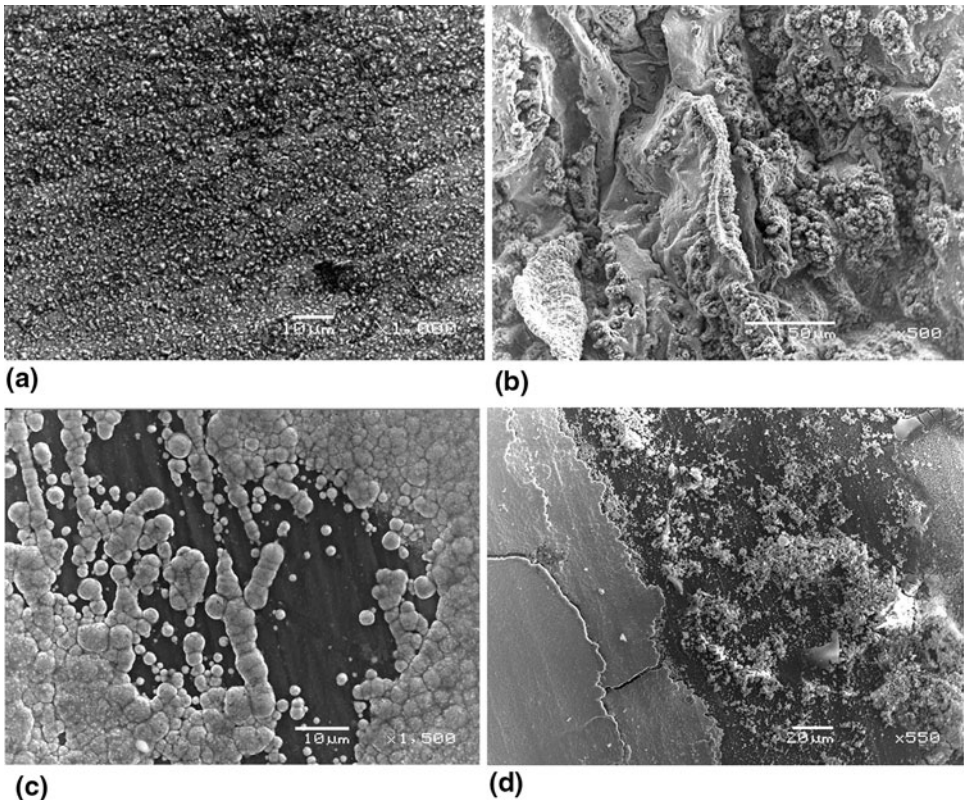

Fig. 1 SEM images of Ni deposit exhibiting various characteristics. (a) Uniform and adherent, (b) non-adherent and curled-up, (c) localized, and (d) cracked and flaky

3.2 Microstructure and Grain Orientation of Ni Electrodeposits

Nickel deposit formed at a constant current density of 50 mA/cm^2 exhibited faceted pyramidal grain structure as shown in the SEM image of Fig. 2(a). This morphology of Ni electrodeposits has been reported in the literature (Ref 17). A decrease in current density to 25 mA/cm^2 results in a decrease in the grain size without changing the grain shape as shown in Fig. 2(b). This is due to the fact that smaller deposition current lowers the depletion of Ni^{2+} ion concentration at the cathode-electrolyte interface resulting in a high nucleation rate on the cathode surface which leads to a small grain size of the deposit (Ref 18–20). The surface of the sample plated at 25 mA/cm^2 was not entirely covered with Ni deposit after 10 min of plating indicating that lower than optimal current density decreases current efficiency. At optimal current density, solubility and electro-conductivity of the electrolyte increases. This enables Ni^{2+} movement and efficient deposition at the cathode surface (Ref 14).

Nickel deposit obtained at a constant voltage of 1.2 V appeared to be an agglomeration of small spheroids with an average size of 100 nm as shown in Fig. 2(c). Sample was not completely covered and revealed regions of bare Al alloy after 5 min of deposition. Current density during deposition varied between 20 and 25 mA/cm^2. Fine crystallite size obtained for this deposit is consistent with relatively lower current density used for deposition. The morphology of Ni deposit obtained under the same conditions but with lesser deposition time of 2 min showed even finer grain size as seen in the SEM micrograph of Fig. 2(d). This indicates that in dc plating the initial deposition of Ni on cathode surface takes the form of fine crystallites. The concentration of Ni^{2+} ions at the cathode-electrolyte interface gradually depletes due to continuous deposition resulting in a progressively coarser grain deposition (Ref 21). Eventually, Ni^{2+} concentration at the interface stabilizes inducing stability in the deposit grain size as well. An AFM image showing the surface topography of fine Ni deposit is shown in Fig. 3. Deposition rate was observed to increase with increased current densities resulting in deposits with a thickness between 7 and 9 μm after 10 min of deposition. Higher current density results in an increase in the rate of Ni^{2+} reduction at cathode surface, thus favoring greater deposition and thicker deposits within the range of current density used in this study.

A STEM cross-sectional bright-field image illustrating typical microstructure of Ni electrodeposit at the interface of substrate and deposit is shown in Fig. 4. It can be seen that Ni grains deposited at the substrate surface at the very beginning of electrodeposition are very fine (≈10 nm). Initially deposited layer is ≈50 nm in thickness. Grain size of Ni present immediately adjacent to this first deposition layer is approximately 50 nm and is seen to become coarser away from the substrate surface. This corroborates earlier suggestion that grain size becomes coarser with deposition time. Microstructure of Ni deposit is primarily composed of high angle grain boundaries. Some grains assume columnar morphology and exhibit twins which is thought to be due to low stacking fault energy exhibited by Ni deposit (Ref 11). Substrate region lying immediately beneath the deposit shows presence of dislocations that might partially be attributed to the stresses generated due to

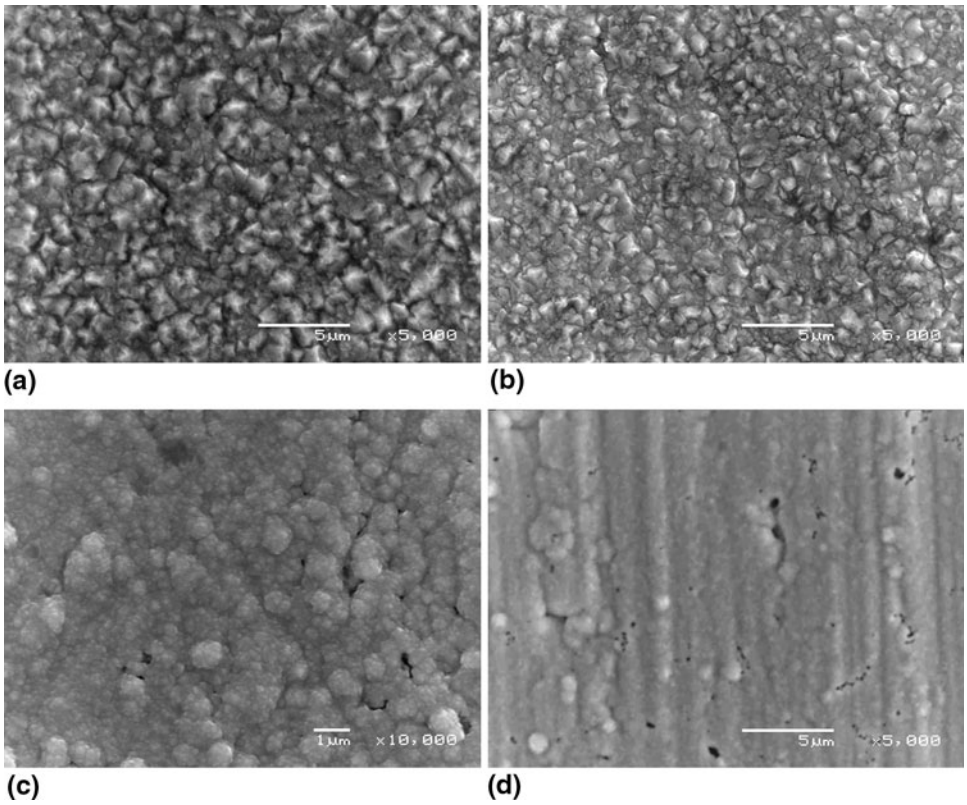

Fig. 2 SEM images of Ni deposit showing relatively (a) coarse and (b) fine, faceted pyramidal morphology (c, d) fine spheroidal grains

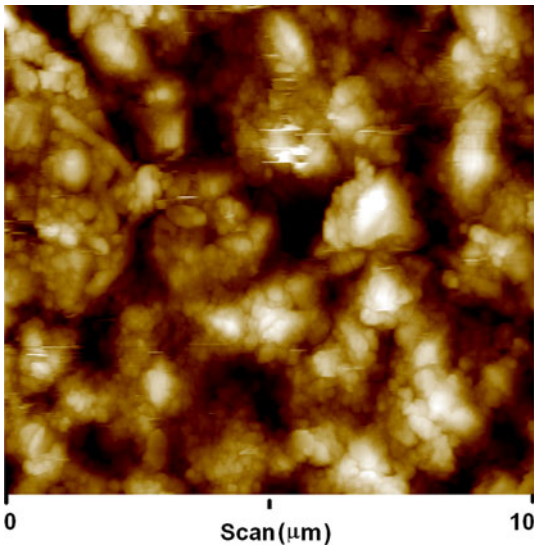

Fig. 3 An AFM image showing fine morphology of Ni deposit

hydrogen evolution during Ni deposition (Ref 15). Grain morphology and texture affect the stability of Ni deposit (Ref 10). Size of grains initially deposited at the cathode surface may influence subsequent grain morphology. Coarse grains may grow at the expense of fine grains during deposition. It was observed in this study that fine-grained Ni deposited initially at the cathode surface generally resulted in adherent and stable deposits overall. This could be partially attributed to low level of porosity associated with fine-grained Ni deposit (Ref 9).

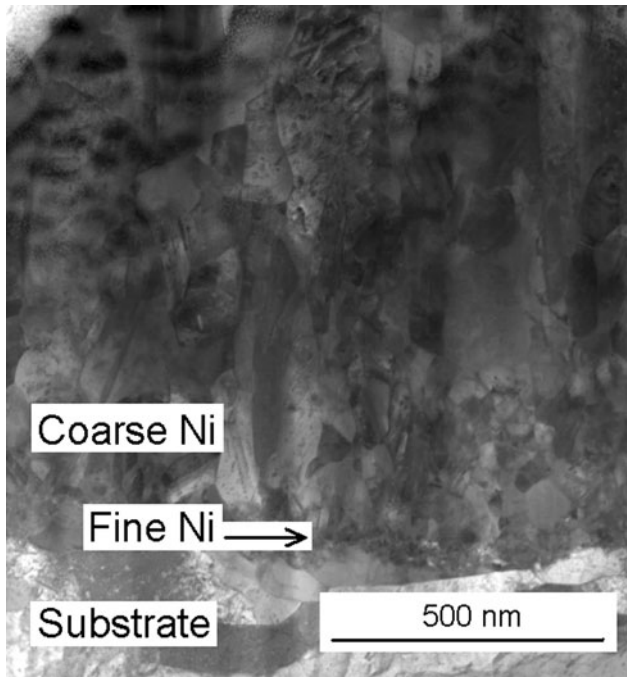

Fig. 4 Cross-sectional STEM bright-field image of Ni deposit showing the formation of a layered structure

X-ray diffraction was used to study the grain orientation of Ni deposits. Figure 5(a) shows a spectrum obtained from Ni deposit that was produced under low current density and exhibited a fine spherical morphology. The peak intensities with

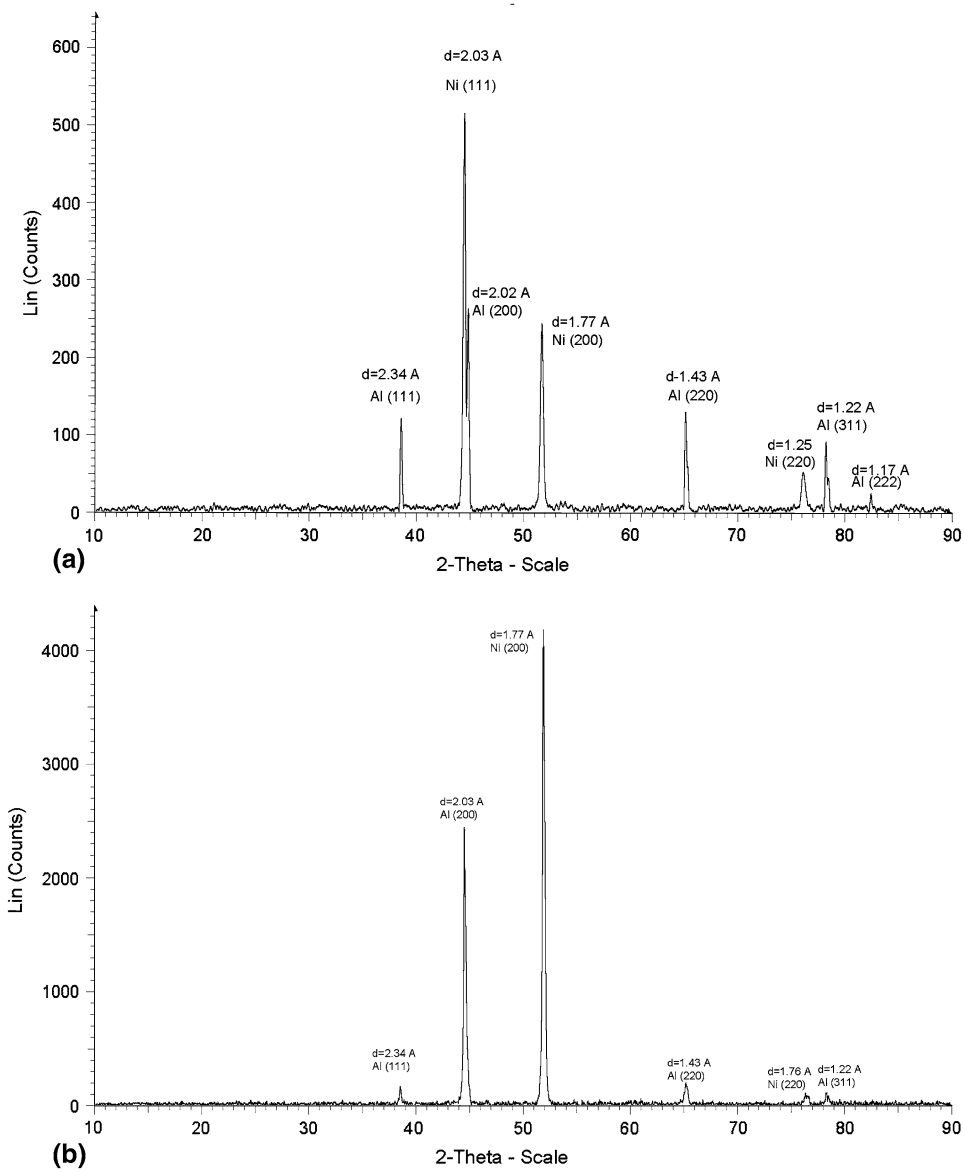

Fig. 5 X-ray diffraction spectra showing (a) random orientation and (b) strong (200) orientation of electrodeposited Ni grains

$I_{(111)} > I_{(200)}$ indicate random grain growth. Deposits that were obtained at higher current density with faceted morphology showed peak intensities with $I_{(200)} > I_{(111)}$ (see Fig. 5b) indicating strong preferred Ni grain growth orientation along [200] direction and perpendicular to (200) planes. This change in orientation of Ni electrodeposits has been reported in literature (Ref 17, 22) and may be attributed to the use of higher current density that may lead to higher electrode overpotential and reduced concentration of Ni^{2+} at the cathode surface giving rise to change in grain size and orientation.

3.3 Microstructure of Heat-Treated Ni Electrodeposits

Al 2014 alloy contains a high density of relatively coarse (≈1-5 μm) second phase particles of $CuAl_2$ as shown in the backscattered electron image of Fig. 6(a). A particle of $CuAl_2$ acts as a local cathode and the surrounding alloy matrix becomes anodic due to depletion in Cu. This results in a galvanic couple that not only promotes electrochemical corrosion but also adversely affects the adhesion of coatings used for protection. The difference in the electrical conductivity between the $CuAl_2$ particles and the alloy matrix produces an inhomogeneous electric field resulting in defects within the protective layer (Ref 23). Second phase particles also affect the deposition and thickening rate of protective coating at localized regions resulting in inhomogeneous growth (Ref 24).

Nickel coated Al 2014 alloy was heat treated to form intermetallics that would serve to improve the adhesion between the Ni deposit and Al alloy substrate. Samples were heated to 520 °C for 10 h in a tube furnace under argon atmosphere followed by water quenching. This was followed by aging process at 170 °C for 10 h under argon followed by furnace cooling in the cold zone (Ref 23). First heat treatment forms intermetallics between Al alloy and the Ni deposit. Second heat treatment serves to recover the hardness of the Al alloy substrate. The morphology of faceted/pyramidal Ni deposit after heat treatment is shown in the SEM image of Fig. 6(b). The faceted microstructure is diluted and relatively

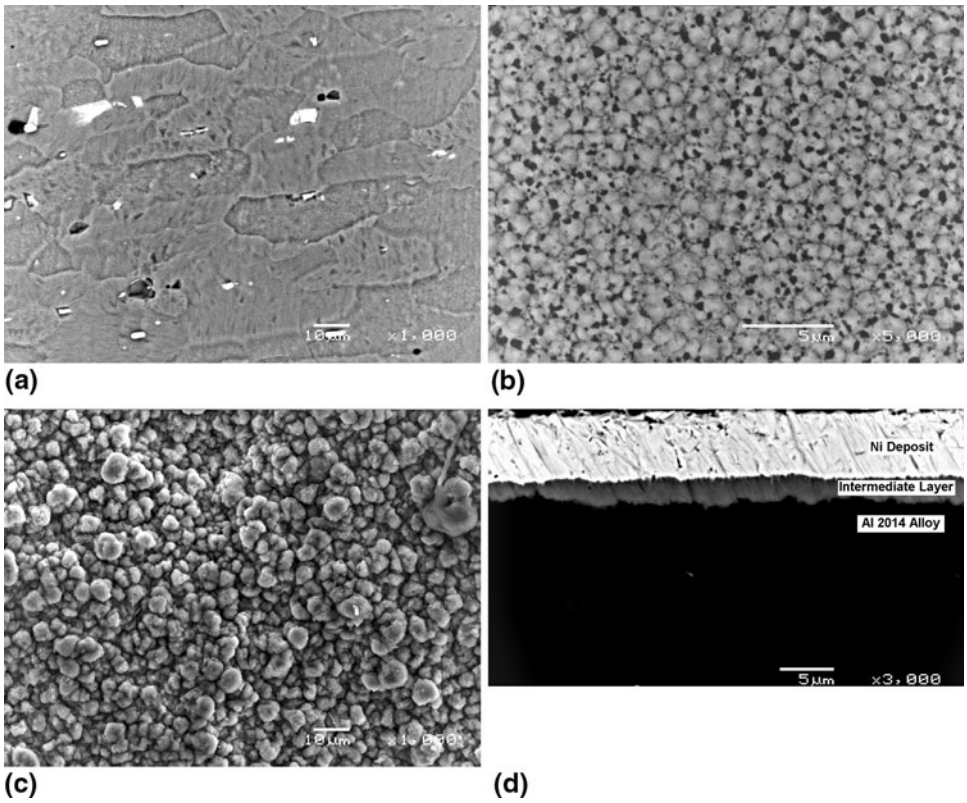

Fig. 6 SEM images showing (a) $CuAl_2$ particles present in Al 2014 alloy and surface morphology of (b) faceted and (c) spheroidal, Ni deposit after heat treatment. (d) Cross-sectional view showing formation of Ni-Cu-Al intermediate layer between the Ni deposit and Al 2014 after heat treatment

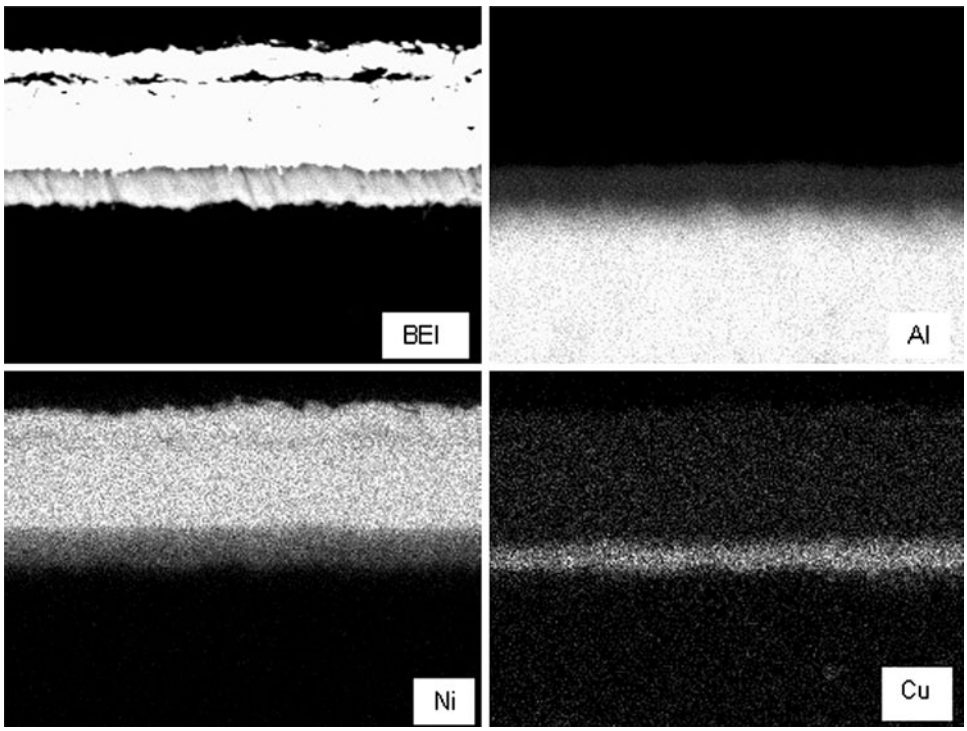

Fig. 7 SEM x-ray mapping images of coating formed on the heat treated sample showing the distribution of Al, Ni, and Cu

coarse voids appear between Ni grains after heat treatment. Figure 6(c) shows the post-heat treatment grain morphology of Ni deposit formed as spheroidal agglomerates. Deposit sustains its spherical morphology and appears to have coarsened to some extent.

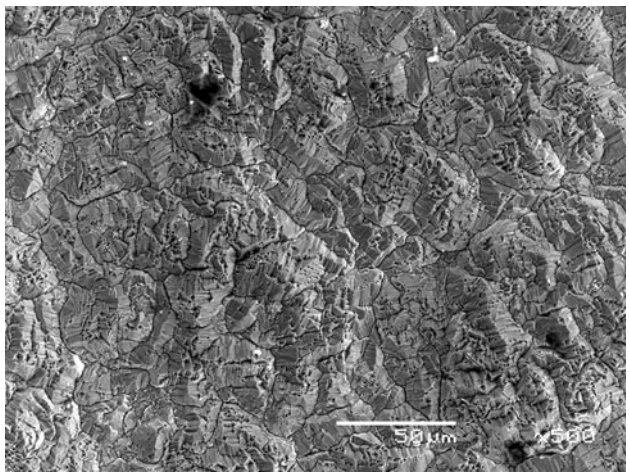

Fig. 8 SEM micrograph of a fracture surface of Ni deposit revealing brittle morphology of Ni-Cu-Al-based intermetallics

An intermediate layer between Ni deposit and the underlying substrate is formed due to heat treatment, as shown in the cross-sectional view of heat-treated sample in Fig. 6(d). Thickness of the intermediate layer was 3 µm and it comprised varying amounts of Ni, Al, and Cu depending on the location of microanalysis within the layer. X-ray mapping images of the heat-treated sample illustrating the distribution of Al, Ni, and Cu are shown in Fig. 7. Typical composition closer to the Ni deposit was 59 wt.% Ni, 36 wt.% Al, and 5 wt.% Cu and near to the Al alloy was 39 wt.% Ni, 38 wt.% Al, and 23 wt.% Cu. The SEM/EDS microchemical analysis indicates that the intermediate layer is composed primarily of Al-Ni type intermetallics such as Al_3Ni, Al_3Ni_2, NiAl, Ni_3Al closer to the Ni deposit and Al-Cu-Ni intermetallics of the type $Al_3(Cu,Ni)_2$, etc., closer to the Al 2014 alloy (Ref 23). The alloy regions immediately beneath the layer were denuded of Cu down to 2.4 wt.%. Intermetallic Al-Cu-Ni exhibited varying hardness with a maximum of 840 VHN at one region. An image of fracture surface obtained from within the intermediate intermetallic layer shows a brittle morphology in Fig. 8. It is believed that formation of intermetallics due to inter-diffusion of elements during heat treatment leads to an increased

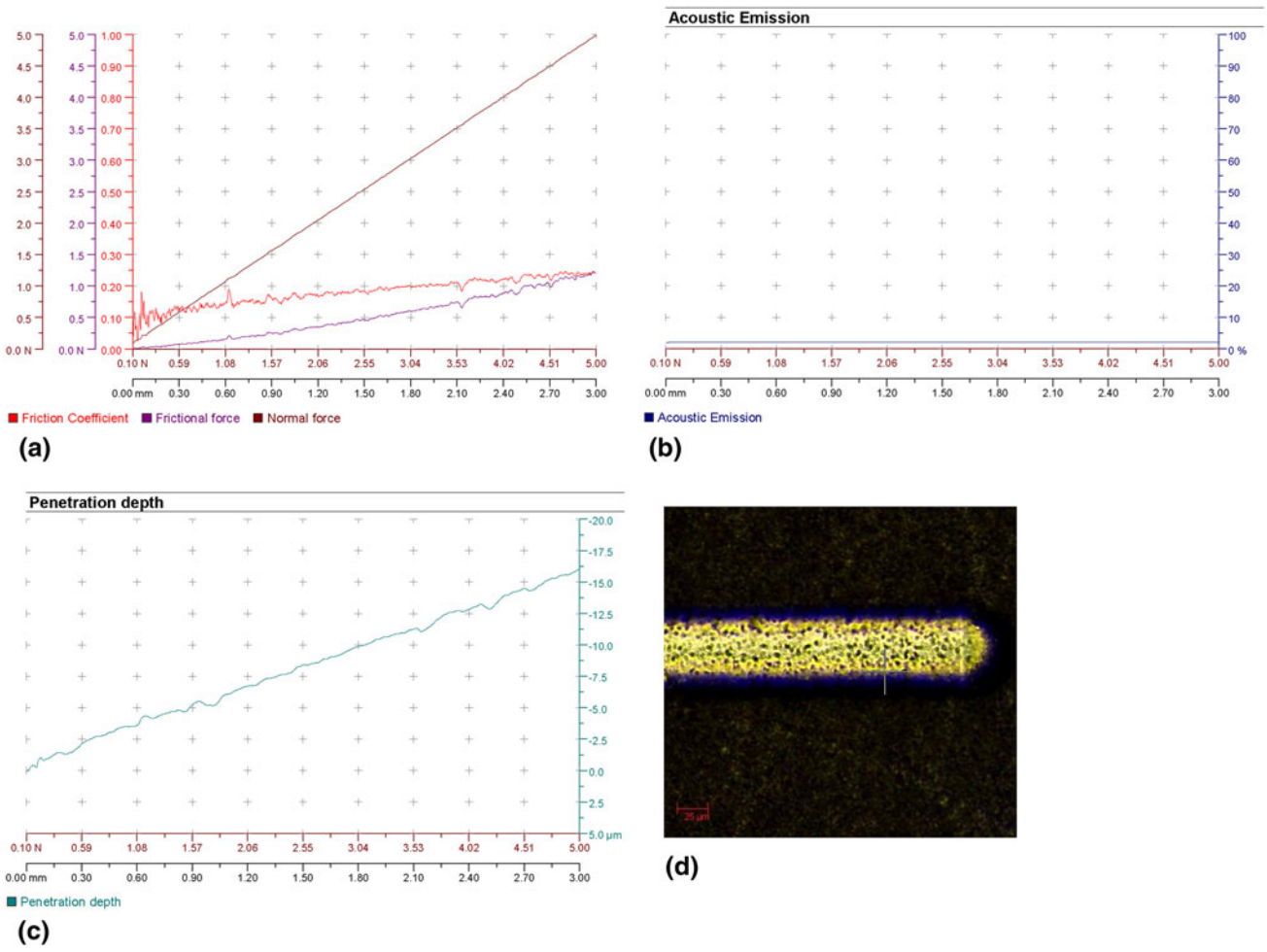

Fig. 9 Microscratch test conducted on Ni deposit at a progressive maximum load of 30 N. (a) Normal force, friction force and coefficient of friction, (b) acoustic emission, and (c) penetration depth are shown plotted with respect to the length of scratch. Lack of signal in the acoustic emission graph indicates that the deposit did not crack or lose its cohesion as also corroborated by the optical image of scratch (d)

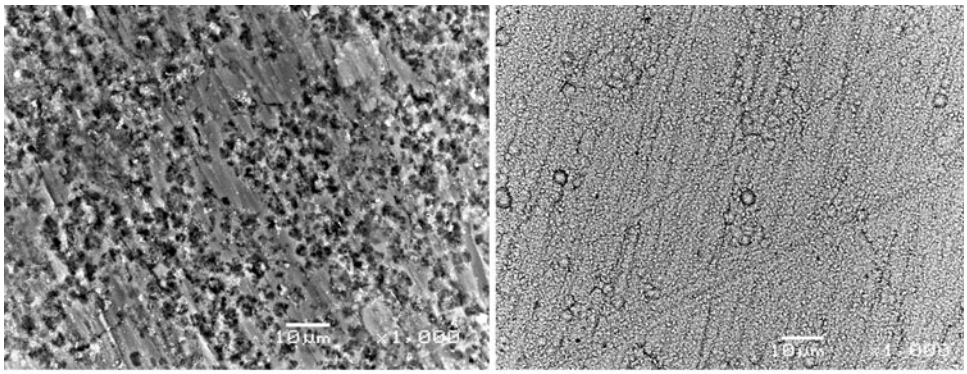

Fig. 10 SEM images of corrosion tested surfaces of (a) Al 2014 showing degradation and (b) Ni deposit where degradation is not apparent

adhesion between Ni deposit and the underlying Al alloy substrate.

3.4 Improvement in Adhesion of Ni Electrodeposits

Heat treatment resulted in a measureable improvement in the adhesion of Ni deposits to the underlying Al 2014 alloy. The microscratch test was used to check the adhesion and fracture characteristics of Ni deposit. A Rockwell indenter was pressed against the moving surface of Ni deposit under a progressive normal load varying from 0.1 to 30 N. This introduces stresses at the interface between the Ni deposit and Al 2014 which can cause cracking, flaking or chipping of the deposit. The microscratch results are shown in Fig. 9(a) to (d). Normal force, friction force, and coefficient of friction are plotted with respect to displacement in Fig. 9(a). Plots for acoustic emission and penetration depth are shown in Fig. 9(b) and (c), respectively. The acoustic emission signal is flat indicating that cracking of deposit does not occur even at a high load of 30 N used for this test. This is corroborated by light microscope picture (see Fig. 9d) showing part of the scratch region where the load was maximum. Cracking or de-cohesion of the Ni deposit was not observed. Preliminary corrosion tests indicated that bare Al 2014 alloy suffered uniform corrosion (see Fig. 10a) in 3.5 wt.% NaCl solution, while surface of the Ni deposit remained undamaged (see Fig. 10b).

4. Conclusions

Uniform, shining, and adherent deposits were obtained on samples with 1 μm surface finish with bath solution pH of 3.6 and a constant current density of 50 mA/cm^2 at 45 °C. Lower deposition current yielded finer Ni grains with spherical morphology. Higher current densities produced faceted and pyramidal Ni grains. Higher currents favored growth of Ni deposits in (200) orientation. Heat treatment improved the adhesion of Ni deposits to the Al alloy by forming an intermediate layer consisting of Ni-Al and Al-Cu-Ni intermetallics. Nickel deposits showed higher hardness and better corrosion behavior when compared to bare Al 2014. It is suggested that electrodeposition of Ni followed by heat treatment can prove to be a viable method to enhance surface properties of Al alloys.

Acknowledgments

The authors wish to acknowledge the support of Center of Research Excellence in Corrosion (CoRE-C), Ministry of Higher Education and the Research Institute at the King Fahd University of Petroleum & Minerals, Dhahran, Saudi Arabia.

References

1. P. Hagans and C.M. Haas, Influence of Metallurgy on the Protective Mechanism of Chromium-Based Conversion Coatings on Aluminum-Copper Alloys, *Surf. Interface Anal.*, 1994, **21**, p 65–78
2. A.K. Mishra and R. Balasubramaniam, Corrosion Inhibition of Aluminum Alloy 2014 by Rare Earth Chlorides, *Corros. Sci.*, 2007, **49**, p 1027–1044
3. Y. Odani, Aluminium Alloys, *Met. Powder Rep.*, 1994, **49**, p 36–40
4. M.J. Ghazali, Wear Characteristic of Several Commercial Wrought Aluminium Alloys Against Tool Steel, *J. Kejuru.*, 2006, **18**, p 49–56
5. D. Pletcher and F.C. Walsh, *Industrial Electrochemistry*, 2nd ed., Chapman and Hall, London, 1990
6. J.K. Dennis and T.E. Such, *Nickel and Chromium Plating*, Butterworth, London, 1986
7. C.P. Steffani, J.W. Dini, J.R. Groza, and A. Palazoglu, Electrodeposition and Corrosion Resistance of Ni-W-B Coatings, *J. Mater. Eng. Perform.*, 1997, **6/4**, p 413–416
8. F. Cai, X. Huang, Q. Yang, and D. Nagy, Effect of Microstructure on the Solid Particle Erosion Properties of Ni Plating, *J. Mater. Eng. Perform.*, 2009, **18/3**, p 305–311
9. V.F.C. Lins, E.S. Cecconello, and T. Matencio, Effect of the Current Density on Morphology, Porosity, and Tribological Properties of Electrodeposited Nickel on Copper, *J. Mater. Eng. Perform.*, 2008, **17/5**, p 741–745
10. U. Klement, L. Hollang, S.R. Dey, M. Battabyal, O.V. Mishin, and W. Skrotzki, Effect of Annealing on Microstructural Development and Grain Orientation in Electrodeposited Ni, *Texture and Anisotropy of Polycrystals III*, Solid State Phenomena Series, Vol 160, Trans Tech Publications Inc., Stafa-Zurich, Switzerland, 2010, p 235-240
11. G.Z. Meng, F.L. Sun, Y.W. Shaoa, T. Zhang, F.H. Wang, C.F. Dong, and X.G. Li, Effect of Phytic Acid on the Microstructure and Corrosion Resistance of Ni Coating, *Electrochim. Acta*, 2010, **55/20**, p 5990–5995
12. M.M. Kamel, Z.M. Anwer, I.T. Abdel-Salam, and I.S. Ibrahim, Nickel Electrodeposition from Novel Lactate Bath, *Trans. Inst. Met. Finish.*, 2010, **88**(4), p 191–197
13. A. Shibata, H. Noda, M. Sone, and Y. Higo, Microstructural Development of an Electrodeposited Ni Layer, *Thin Solid Films*, 2010, **518**(18), p 5153–5158
14. J.X. Kang, W.Z. Zhao, and G.F. Zhang, Influence of Electrodeposition Parameters on the Deposition Rate and Microhardness of Nanocrystalline Ni Coatings, *Surf. Coat. Technol.*, 2009, **203**(13), p 1815–1818

15. A.M. El-Sherik, J. Shirokoff, and U. Erb, Stress Measurements in Nanocrystalline Ni Electrodeposits, *J. Alloys Compd.*, 2005, **389**, p 140–143
16. M. Holm and T.J. O'Keefe, Evaluation of Nickel Deposition by Electrochemical Impedance Spectroscopy, *J. Appl. Electrochem.*, 2000, **30**, p 1125–1132
17. A.M. El-Sherik, U. Erb, and J. Page, Microstructural Evolution in Pulse Plated Nickel Electrodeposits, *Surf. Coat. Technol.*, 1996, **88**, p 70–78
18. E. Toth-Kadar, I. Bakonyi, L. Pogany, and A. Cziraki, Microstructure and Electrical Transport Properties of Pulsed-Plated Nanocrystalline Nickel Electrodeposits, *Surf. Coat. Technol.*, 1997, **88**, p 57–65
19. I. Bakonyi, E. Toth-Kadar, L. Pogany, A. Cziraki, I. Gerocs, K. Varga-Josepovits, B. Arnold, and K. Wetzig, Preparation and Characterization of d.c.-Plated Nanocrystalline Nickel Electrodeposits, *Surf. Coat. Technol.*, 1996, **78**, p 124–136
20. D.-T. Chin, Mass Transfer and Current-Potential Relation in Pulse Electrolysis, *J. Electrochem. Soc.*, 1983, **130**, p 1657–1667
21. A. Cziraki, I. Gerocs, B. Fogarassy, E. Toth-Kadar, and I. Bakonyi, Microstructure and Growth of Electrodeposited Nanocrystalline Nickel Foils, *J. Mater. Sci.*, 1994, **29**, p 4771–4777
22. Y. Xuetao, W. Yu, S. Dongbai, and Y. Hongying, Influence of Pulse Parameters on the Microstructure and Microhardness of Nickel Electrodeposits, *Surf. Coat. Technol.*, 2008, **202**, p 1895–1903
23. J.M. Molina, R.A. Saravanan, J. Narciso, and E. Louis, Surface Modification of 2014 Aluminium Alloy–Al_2O_3 Particles Composites by Nickel Electrochemical Deposition, *Mater. Sci. Eng.*, 2004, **383**, p 299–306
24. Y. Liu, P. Skeldon, G.E. Thompson, H. Habazaki, and K. Shimizu, Chromate Conversion Coatings on Aluminium-Copper Alloys, *Corros. Sci.*, 2005, **47**, p 341–354